Ultra-Low Thermal Conductivity of Atomic/Molecular Layer-Deposited Hybrid Organic-Inorganic Zincone Thin Films.

ARTICLE *in* NANO LETTERS · OCTOBER 2013

Impact Factor: 13.59 · DOI: 10.1021/nl403244s · Source: PubMed

NANO LETTERS

Letter

pubs.acs.org/NanoLett

Ultralow Thermal Conductivity of Atomic/Molecular Layer-Deposited Hybrid Organic–Inorganic Zincone Thin Films

Jun Liu,[†] Byunghoon Yoon,[‡] Eli Kuhlmann,[†] Miao Tian,[†] Jie Zhu,[§] Steven M. George,[†,‡] Yung-Cheng Lee,[†] and Ronggui Yang*[,†]

[†]Department of Mechanical Engineering, University of Colorado, Boulder, Colorado, 80309, United States

[‡]Department of Chemistry and Biochemistry, University of Colorado, Boulder, Colorado, 80309, United States

[§]Institute of Engineering Thermophysics, Chinese Academy of Sciences, Beijing, 100190, China

Supporting Information

ABSTRACT: Atomic layer deposition (ALD) and molecular layer deposition (MLD) techniques with atomic level control enable a new class of hybrid organic–inorganic materials with improved functionality. In this work, the cross-plane thermal conductivity and volumetric heat capacity of three types of hybrid organic–inorganic zincone thin films enabled by MLD processes and alternate ALD–MLD processes were measured using the frequency-dependent time-domain thermoreflectance method. We revealed the critical role of backbone flexibility in the structural morphology and thermal conductivity of MLD zincone thin films by comparing the thermal conductivity of MLD zincone films with an aliphatic backbone to that with aromatic backbone. Much lower thermal conductivity values were obtained in ALD/MLD-enabled hybrid organic–inorganic zincone thin films compared to that of the ALD-enabled W/Al_2O_3 nanolaminates reported by Costescu et al. [*Science* **2004**, *303*, 989–990], which suggests that the dramatic material difference between organic and inorganic materials may provide a route for producing materials with ultralow thermal conductivity.

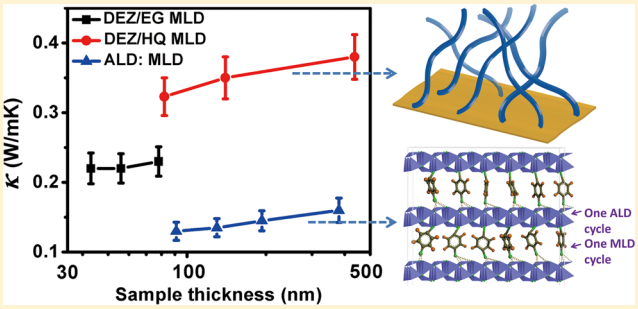

KEYWORDS: *Atomic layer deposition, molecular layer deposition, hybrid organic–inorganic material, thermal conductivity*

Atomic layer deposition (ALD)[1] and molecular layer deposition (MLD)[2] have received great attention over the past two decades for the fabrication of ultrathin functional materials with atomic level control for various applications such as low leakage dielectric films, diffusion barrier coatings, and transparent conducting coatings.[3] When alternated, ALD/MLD utilizing sequential and self-limiting surface reactions can enable a new class of hybrid organic–inorganic materials with enhanced electrical, optical, magnetic, and mechanical properties compared to conventional organic or inorganic materials.[4,5] As an example, hybrid zinc alkoxide (or zincone) thin films have recently been fabricated using an alternate ALD/MLD process and demonstrated as a promising candidate for transparent conducting coatings.[6] The composition and thickness of each individual inorganic/organic layer in these zincone films can be controlled by the ALD/MLD cycles.[2,3,7−13] The heterogeneous interatomic/molecular bonding and mass difference between organic molecules and inorganic atoms in these zincone thin films can significantly inhibit the phonon transport and reduce the thermal conductivity to be much lower than their inorganic and organic counterparts.[14−16] As a result, such ALD/MLD-enabled hybrid organic–inorganic materials could be promising thermal insulation materials or even high-efficiency thermoelectric materials due to the expected low thermal conductivity.[17−19]

In this Letter, we study for the first time the thermal conductivity and volumetric heat capacity of such novel ALD/MLD-enabled hybrid organic–inorganic zincone thin films to investigate the effect of atomic configuration and structural morphology on the thermal properties of ALD/MLD-enabled hybrid organic–inorganic materials.

Three sets of hybrid organic–inorganic zincone thin films were prepared based on zinc precursors and organic diols on p-type (100) Si wafers.[9] A 1 nm alumina layer was deposited first by ALD at 150 °C as the adhesion layer that promotes the initial ALD/MLD growth. Diethyl zinc (DEZ) can react with aliphatic organic diols such as ethylene glycol (EG) or aromatic organic diols such as hydroquinone (HQ), which forms type A and type B MLD zincone films, respectively.[3] Figure 1a and b shows the schematic drawing of type A and type B MLD zincone films, which are fabricated with DEZ/EG (1:1) and DEZ/HQ (1:1) in sequence. ZnO can be deposited using ALD with DEZ and H_2O as the reactants. By alternating ZnO ALD and zincone MLD, the type C ALD–MLD zincone film is fabricated with DEZ/H_2O (1:1) and DEZ/HQ (1:1) in sequence, as shown in Figure 1c. Details on the chemical

Received: August 29, 2013
Revised: October 26, 2013
Published: October 28, 2013

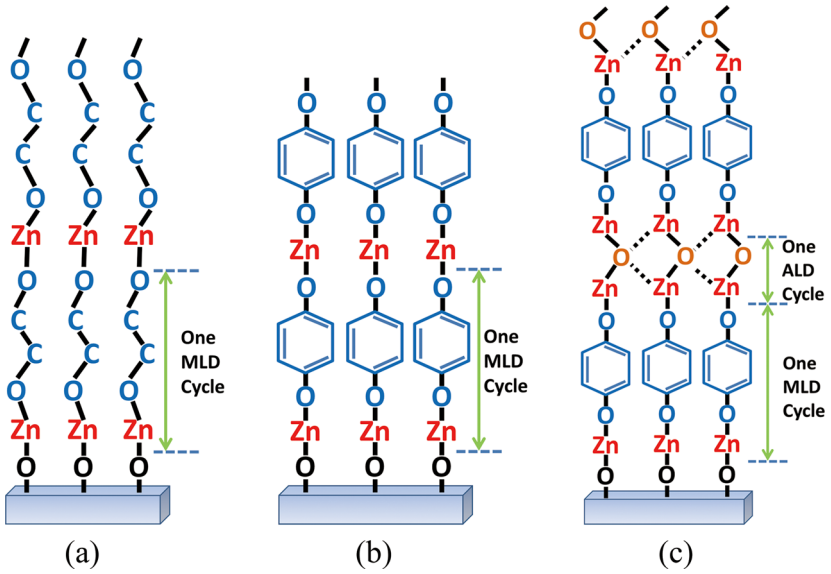

Figure 1. (a) Schematic drawing of MLD cycles for type A MLD zincone film using diethyl zinc (DEZ) and ethylene glycol (EG). (b) Schematic drawing of MLD cycles for type B MLD zincone film using DEZ and hydroquinone (HQ). (c) Schematic drawing of type C ALD−MLD zincone film deposited using DEZ/H_2O and DEZ/HQ in sequence.

reactions, the fabrication procedures, and fabrication conditions of zincone thin film samples studied in this work can be found in literature[3,6,9] and in Section I of the Supporting Information.

By varying MLD or ALD−MLD cycle numbers, three sets of type A, type B, and type C zincone films with various thicknesses have been fabricated, as listed in Table 1. The

Table 1. Three Sets of Type A, Type B, and Type C Zincone Thin Films with Various Thicknesses Fabricated with Different MLD and ALD−MLD Cycles and Cycle Numbers[a]

type	one cycle	thickness (nm)	cycle number	average growth rate (nm/cycle)
A	DEZ/EG	43	500	0.086
A	DEZ/EG	56	1000	0.056
A	DEZ/EG	78	2000	0.039
B	DEZ/HQ	82	300	0.273
B	DEZ/HQ	136	500	0.272
B	DEZ/HQ	437	1600	0.273
C	DEZ/H_2O/DEZ/HQ	91	600	0.152
C	DEZ/H_2O/DEZ/HQ	139	900	0.154
C	DEZ/H_2O/DEZ/HQ	193	1300	0.148
C	DEZ/H_2O/DEZ/HQ	380	2500	0.152

[a]The average growth rate is estimated by dividing the thickness of each film with the cycle number.

thickness of the zincone thin films was measured by the X-ray reflectometry (XRR) using a Bede D1 diffractometer and confirmed by scanning electron microscope (SEM) cross-sectional images after the sample was milled by focused ion beam (FIB) in a Nova 600i dual beam FIB instrument. As an example, Figure 2a shows the cross-sectional SEM image with a 52° tilted view of a 436.8 nm thick type B MLD zincone film on a p-type (100) Si wafer after a trench was milled using FIB. Grazing incidence X-ray diffraction (GIXRD) data using the Bede D1 diffractometer were used to qualitatively analyze the atomic crystallographic order of these zincone films. Figure 2b shows the GIXRD data of 43 nm thick type A MLD zincone film, 136 nm thick type B MLD zincone film, and 139 nm thick

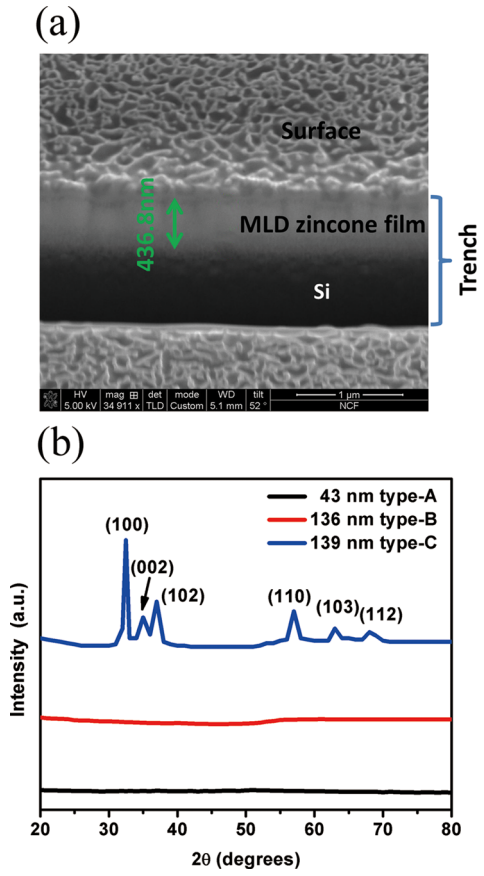

Figure 2. (a) Cross-sectional scanning electron microscope (SEM) image with a 52° tilted view of a 436.8 nm thick type B MLD zincone film on a (100) Si wafer after a trench was milled using focused ion beam (FIB). (b) GIXRD data of the 43 nm thick type A MLD zincone film, 136 nm thick type B MLD zincone film, and 139 nm thick type C ALD−MLD zincone film.

type C ALD−MLD zincone film. No obvious peaks are observed in the GIXRD data for the 43 nm thick type A and

dx.doi.org/10.1021/nl403244s | Nano Lett. 2013, 13, 5594−5599

136 nm thick type B MLD zincone films, which indicates that these films lack crystalline order. Six peaks appear in the GIXRD data for the 139 nm thick type C ALD−MLD zincone film, which matches with the characteristics of the (100), (002), (102), (110), (103), and (112) crystal planes of ZnO crystal. Each crystal plane direction represents one orientation of the atomic flakes in the ALD ZnO layer. The 139 nm thick type C ALD−MLD film exhibits strong ZnO (100) preferred orientation parallel to the sample surface, which has the strongest signal in the GIXRD data. In these type C ALD−MLD zincone thin films, the atom-thick ZnO flakes fabricated by ALD cycles are connected by the molecular layer-thick HQ enabled by the DEZ/HQ MLD process. Additionally, the areal size of these atom-thick ALD ZnO flakes can be estimated from the Scherrer's formula.[20] The areal size of the (100) oriented atomic flakes with the strongest GIXRD signal is estimated to be about 13 nm, while the size of other flakes are estimated to be about 6−9 nm. A detailed calculation of the areal size is presented in Section II of the Supporting Information.

The cross-plane (through film thickness direction) thermal conductivity and the volumetric heat capacity of zincone thin film samples were simultaneously measured using an ultrafast laser-based time-domain thermoreflectance (TDTR) method.[21−24] The TDTR method has recently emerged as a high-accuracy thermal conductivity measurement technique. Frequency-dependent TDTR measurement has recently been explored by Liu et al.[23] for simultaneous cross-plane thermal conductivity and volumetric heat capacity measurement. Applying this frequency-dependent TDTR technique on these novel zincone samples reduces the measurement uncertainty associated with the volumetric heat capacity, which is otherwise used as input for the measurement. Figure 3a shows the sample configuration for the TDTR measurement (left: zincone sample, right: reference sample). A ∼100 nm thick aluminum (Al) thin film is thermally evaporated on the top as the metal transducer and temperature sensor. The thickness of this metal transducer layer is determined by the acoustic echoes in the TDTR signal. Before thermal evaporation of Al transducer, an 8 nm thick alumina capping layer is deposited using ALD on top of the zincone thin film, which prevents the zincone film from reacting with Al vapor when the Al layer is deposited. The thermal conductance of the alumina capping layers was extracted by measuring the reference samples (on the right) that consist of the Al thin film, an 8 nm thick (or 16 nm thick) alumina layer, and the (100) Si substrate. The frequency-dependent TDTR measurements were carried out at modulation frequencies of 0.5, 0.98, and 6.8 MHz. The details of the experiment setup and the data reduction scheme have been presented in literature[23,25] and also in Section III of the Supporting Information.

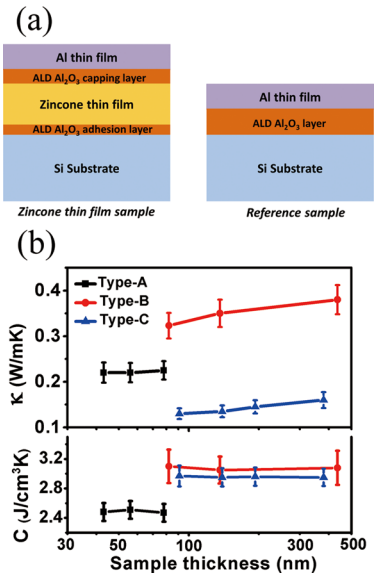

Figure 3. (a) Sample configuration for the TDTR measurement of zincone thin films (left: zincone thin film sample, right: reference sample). (b) Dependence on the sample thickness and chemical composition (film type) of the cross-plane thermal conductivity and volumetric heat capacity of zincone thin films.

Figure 3b shows the dependence on the sample thickness and chemical composition (film type) of the cross-plane thermal conductivity of zincone thin films at room temperature. The thermal conductivity of all three types of zincone thin films increases only slightly with film thickness, which is attributed to the structural morphology, since a length-dependent thermal conductivity would have been observed if the MLD chains are vertically aligned.[26,27] The thermal conductivity of type B MLD zincone films with the DEZ/HQ sequence is higher than that of type A MLD zincone films with the DEZ/EG sequence. The thermal conductivity of the type C ALD−MLD-enabled films with an alternate DEZ/H_2O sequence and DEZ/HQ sequence is much lower, which is only around 1/3 that of type B MLD zincone films.

Table 2 shows the mass density, the average growth rate, the idealized linear growth rate, and the estimated reactive site density during the growth of the 43 nm thick type A MLD zincone film, 136 nm thick type B MLD zincone film, and 139 nm thick type C ALD−MLD zincone film, with the details described in section IV of the Supporting Information. The mass density of each film is calculated by the total mass gain measured using the in situ quartz crystal microbalance (QCM) divided by the film thickness measured using by XRR. Apparently the measured average growth rate or deposition rate, which is the increase of the thin film thickness per deposition cycle, is much smaller than the idealized linear growth rate (molecular length per cycle). This indicates that the orientation of the backbone of molecular chain segments is randomly distributed rather than the hypothesized vertical alignment of MLD cycles. Such a randomly distributed orientation of MLD chains is likely the reason for the weak

Table 2. Mass Density, Average Growth Rate, Idealized Linear Growth Rate, and Estimated Reactive Site Density of the 43 nm Thick Type A MLD Zincone Film, 136 nm Thick Type B MLD Zincone Film, and 139 nm Thick Type C ALD−MLD Zincone Film

	density (g/cm^3)	average growth rate (nm/cycle)	idealized linear growth rate (nm/cycle)	estimated reactive site density
43 nm thick type A	1.9	0.086	∼0.69	36.4%
136 nm thick type B	1.9	0.272	∼0.84	98.1%
139 nm thick type C	5.0	0.154	∼1.06	N/A

dx.doi.org/10.1021/nl403244s | Nano Lett. 2013, 13, 5594−5599

dependence of thermal conductivity on the thickness as observed in Figure 3b.

The key difference between type A and type B MLD zincone films is the organic component with aliphatic (EG) or aromatic (HQ) backbone, which has a very different rotational energy barrier or flexibility. It is easier for the aliphatic backbone in type A MLD zincone films to change its conformation by rotating to reach the minimum energy due to the lower rotational energy barrier than that of aromatic backbone in type B MLD zincone films. This difference in rotational energy barriers would result in more "double reactions" during the deposition process of type A MLD zincone films using DEZ and EG than that of type B MLD zincone films using DEZ and HQ, where both hydroxyl moieties (−OH) in the EG molecules react with adjacent surface sites to produce nonreactive Zn−ethylene oxide groups.[3,9] The double reactions in type A MLD zincone films lead to a loss of reactive surface sites or the decrease of reactive site density and produce a less average growth rate during MLD compared to that in the growth of type B MLD zincone films. For instance, the average growth rate for the 43 nm thick type A MLD zincone film is 0.086 nm/cycle, which is much less than the average growth rate 0.272 nm/cycle for the 136 nm thick type B MLD zincone film. The reactive site density in the linear growth region is 98.1% in the 136 nm thick type B MLD zincone film compared to 36.4% in 43 nm thick type A MLD zincone film. In addition, a decreasing average growth rate with increasing film thickness is found in type A MLD zincone films, while the average growth rates in type B MLD zincone films and type C ALD−MLD zincone films are rather constant, as shown in Table 1. Due to the happening of a large number of double reactions, it is rather challenging to grow type A MLD zincone films to exceed 100 nm thick. Figure 4a and b shows the sketches of the structural morphology (atomic configuration and chain orientation) of type A and type B MLD zincone thin films inferred from the estimation of the growth rate, the reactive site density, and the GIXRD data. In both type A and type B MLD zincone films, the hybrid organic−inorganic molecular chains are somewhat tilt-oriented rather than vertically oriented on the deposited surface. However, the molecular chains in type B MLD zincone films are tilted with a slightly larger angle with respect to the surface due to a more rigid aromatic structure using HQ precursor. The percentage of molecular chains in type B MLD zincone films that lie down on the surface is also much less than that in type A MLD zincone film. As a result, thermal conductivity of type B MLD zincone films is larger than that of type A MLD zincone films.

Even though the MLD cycles in the deposition of type C ALD−MLD zincone films are the same as those in the deposition of type B MLD zincone films, the introduction of alternate ALD cycles in the deposition process dramatically changes the atomic configuration of the type C ALD−MLD zincone films. Besides forming the atom-thick ALD ZnO flake, HQ in the MLD cycle can react with both the DEZ in the ALD cycle and the MLD cycle in the growth of type C ALD−MLD zincone film, which results in a much denser film compared to type B MLD zincone film and a much lower average growth rate compared to the idealized linear growth rate, as shown in Table 2. Figure 4c shows the sketch of the atomic configurations of type C ALD−MLD zincone films inferred from the estimation of the growth mechanism and the GIXRD data. In the type C ALD−MLD zincone films, the alternate layers with atom-thick ALD ZnO flake and tilted MLD organic

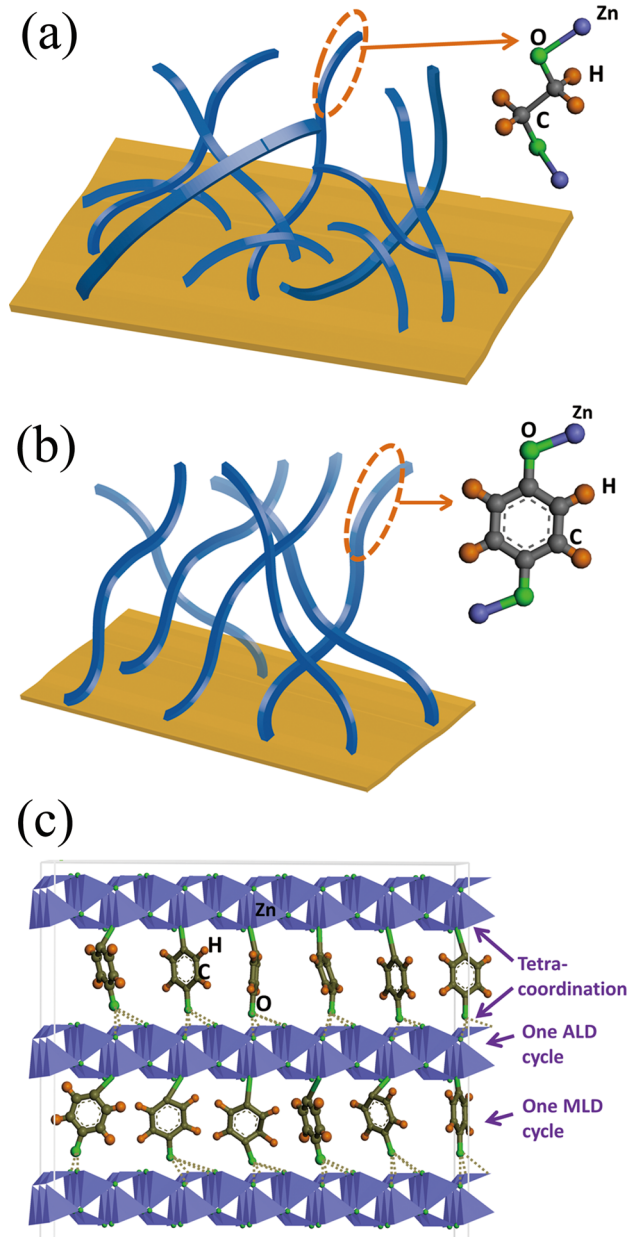

Figure 4. Sketch of structural morphology of (a) type A MLD zincone film, (b) type B MLD zincone film, and (c) type C ALD−MLD zincone film. In a and b, the hybrid organic−inorganic molecular chains are tilt-oriented on the deposited surface rather than vertically oriented on the deposited surface. The alternate layers of atom-thick ALD ZnO flakes and the MLD layer are formed in type C ALD−MLD zincone films (c). The blue atom is Zn, the green atom is O, the orange atom is H, and the gray atom is C. The tetra-coordination formed by the interactions between Zn atoms and adjacent oxygen atoms in type C ALD−MLD zincone films is also marked.

layer are formed, which is very different from the hybrid organic−inorganic molecular chain structure in the type A and type B MLD zincone films as shown in Figure 4a and b. Such an alternate-layer structure with very different atomic configurations between atom-thick ZnO flakes and the molecule chains strongly scatters phonons and reduces the thermal conductivity of the type C ALD−MLD zincone film compared to that of type A and type B MLD zincone films.

In an earlier work by Costescu et al.,[17] the thermal conductivity of 40−70 nm thick (sample thickness) ALD-

dx.doi.org/10.1021/nl403244s | Nano Lett. 2013, 13, 5594−5599

enabled W/Al_2O_3 nanolaminates (electrically nonconductive) deposited by one of the coauthors of the present paper was measured to be 0.6−1.5 W/m·K at room temperature. Here we showed that much lower thermal conductivity values, in the range of 0.13−0.38 W/m·K, are obtained in ALD/MLD-enabled hybrid organic−inorganic zincone thin films, which promises to produce thermal superinsulators. In addition, the type C ALD−MLD zincone thin films, which are electrically conductive,[6] could even be explored as thermoelectric materials.

By assuming perfect layered structures, we can roughly estimate the upper bound of interfacial thermal conductance G_{limit} between the ALD and MLD layers using a simple series resistance model,

$$\frac{d}{\kappa_{film}} = \frac{d_{ALD}}{\kappa_{ALD}} + \frac{1}{G_{limit}} + \frac{d_{MLD}}{\kappa_{MLD}} \quad (1)$$

where κ_{film} is the measured cross-plane thermal conductivity of type C ALD−MLD zincone films and d is the thickness of one ALD/MLD cycle (d = 0.72 nm). The thickness of ALD layer d_{ALD} is 0.45 nm, which is calculated from the atomic structure of ZnO. The thickness of MLD layer d_{MLD} is 0.27 nm, assuming that the growth rate of the same MLD layer in the type C ALD−MLD zincone film is the same to that measured in the type B MLD zincone film. The thermal conductivity of ALD ZnO layer κ_{ALD} is taken as 2.3 W/m·K.[28] The thermal conductivity of MLD layer κ_{MLD} is estimated to be the same as poly(phenylene ester) (0.22 W/m·K).[29] We note that this estimation is the upper bound because the ZnO forms flake-like structure in type C ALD−MLD zincone films and there were indeed much less interfaces formed in the materials than perfect layering shown in Figure 4.[30] The upper bound of the interfacial thermal conductance G_{limit} between the ALD and the MLD layer in the four samples of type C ALD−MLD zincone films is estimated to be 243−325 MW/m^2·K at 300 K. This value is consistent with that across the organic−inorganic interfaces measured in organoclay nanolaminates by Lesego et al.[31] (150−240 MW/m^2·K) and colloidal nanocrystal arrays by Ong et al.[32] (140 MW/m^2·K). Compared to the interfacial thermal conductance between ALD inorganic W and Al_2O_3 layers, 260 MW/m^2·K, estimated by Costescu et al.,[17] all of these reports showed a much smaller thermal conductance across the organic−inorganic interface due to the drastic difference in phonon spectra in organic and inorganic materials.

Figure 5 shows the temperature dependence of volumetric heat capacity and thermal conductivity for a 78 nm thick type A MLD zincone film, a 82 nm thick type B MLD zincone film, and a 91 nm thick type C ALD−MLD zincone film. Figure 5a shows that the volumetric heat capacity of all three types of zincone thin films increases with temperature first since more phonon modes with higher frequencies are excited at elevated temperatures and finally levels off at a temperature higher than 250 K, which is a very typical behavior of solids.[33,34] Although not calculated in this work, the phonon modes of the organic components in zincone thin films can be assumed to be similar to that in poly(ethylene oxide) (for type A MLD zincone film) or poly(phenylene ether) (for type B MLD zincone films and type C ALD−MLD zincone films), where there are much less phonon modes in the range of 5−10 THz than those in the range of 0−5 THz for both polymers, as calculated from lattice dynamics simulations.[35] The phonon modes with frequencies above 5 THz can be thermally activated at a temperature higher than 250 K (calculated from $h\nu/k_B$, where h is the Planck constant, ν is the phonon frequency, κ_B is the Boltzmann constant). However, due to the limited number of the modes, the contribution to the heat capacity increase in the temperature range of 250−400 K is small. To understand the effect of structure on heat capacity, the specific heat capacity C_p (per gram) is calculated by dividing the measured volumetric heat capacity by the mass density shown in Table 2. At room temperature, the specific heat capacity of type A (1.316 J·g^{-1}·K^{-1}) and type B (1.605 J·g^{-1}·K^{-1}) MLD zincone films is close to that of their organic counterparts, poly(ethylene oxide) (1.136 J·g^{-1}·K^{-1})[36] and poly(phenylene oxide) (1.204 J·g^{-1}·K^{-1}).[37] However, the specific heat capacity of type C ALD−MLD zincone films, 0.590 J·g^{-1}·K^{-1}, is much closer to that of their inorganic counterparts, zinc oxide (0.460 J·g^{-1}·K^{-1}),[38] which further confirms the different structural morphology of type C ALD−MLD zincone thin films from that of type A and type B MLD zincone thin films. Figure 5b shows that the thermal conductivity increases with increasing temperature from 150 to 400 K for type A and type B MLD zincone films, which is very similar to the temperature-dependent thermal conductivity of amorphous materials.[39,40] However, a temperature dependence trend similar to that of crystalline materials was observed in the thermal conductivity of the type C ALD−MLD zincone thin films. The thermal conductivity increases from 150 to 300 K due to the rapid increase of heat capacity and then slightly decreases with a temperature from 300 to 400 K. The temperature dependence observed in Figure 5 further confirms the crystalline-nature structural morphology shown in Figure 4.

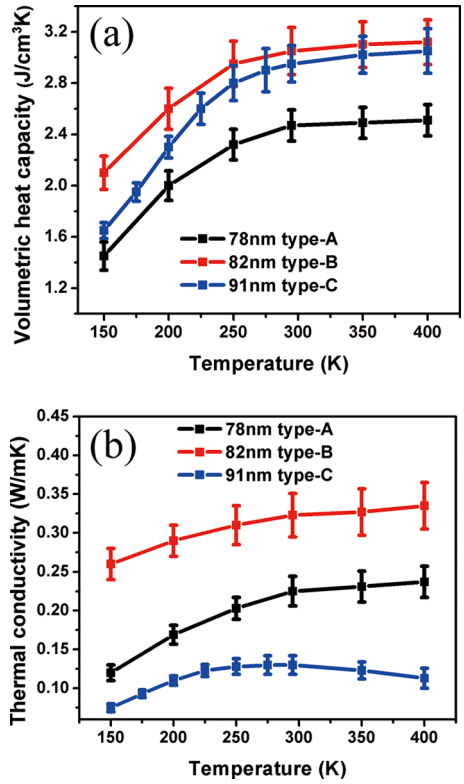

Figure 5. Temperature dependence of (a) volumetric heat capacity and (b) thermal conductivity of a 78 nm thick type A MLD zincone film, a 82 nm thick type B MLD zincone film, and a 91 nm thick type C ALD−MLD zincone film.

dx.doi.org/10.1021/nl403244s | Nano Lett. 2013, 13, 5594−5599

In summary, the cross-plane thermal conductivity and volumetric heat capacity of hybrid organic−inorganic zincone thin films enabled by MLD processes and alternate ALD−MLD processes were measured using the frequency-dependent TDTR method. The thermal conductivity of MLD zincone film with DEZ/HQ sequence is higher than that of MLD zincone film with DEZ/EG sequence, due to the critical role of flexibility that the backbones (EG or HQ) play in the structural morphology and thermal conductivity of the zincone thin films. In the ALD−MLD zincone film, the alternate-layering structure with very different atomic configurations between the ALD atomic flake layers and the MLD molecular layers strongly scatters phonons, which reduces the thermal conductivity to be much lower than that of the MLD zincone films with the same organic component. Much lower thermal conductivity values are obtained in ALD/MLD-enabled hybrid organic−inorganic zincone thin films compared to that of the ALD-enabled W/Al_2O_3 nanolaminates reported by Costescu et al.,[17] which suggests that the dramatic material difference between organic and inorganic materials may provide a route for producing materials with ultralow thermal conductivity.

■ ASSOCIATED CONTENT

Supporting Information

Detailed sample fabrication process of zincone thin films, the analysis of the atomic configurations of the zincone thin films, and the detailed measurement method for thermal properties. This material is available free of charge via the Internet at http://pubs.acs.org.

■ AUTHOR INFORMATION

Corresponding Author

*Tel: +1-303-735-1003. Fax: +1-303-492-3498. E-mail: ronggui.yang@colorado.edu.

Notes

The authors declare no competing financial interest.

■ ACKNOWLEDGMENTS

The authors would like to thank Younghee Lee, Virginia Anderson, and Daniel Higgs for helpful discussions. This work was supported by the DARPA Thermal Ground Plane Program (contract no. N66001-08-C-2006), AFOSR Award (Grant No. FA9550-11-1-0109), and NSF CAREER Award (grant no. 0846561). J.Z. would like to acknowledge the support from National Natural Science Foundation of China (grant no. 51206167). The metal transducer microfabrication described in this work was conducted in the Colorado Nanofabrication Laboratories, which is supported by the NNIN and the National Science Foundation under grant no. ECS-0335765.

■ REFERENCES

(1) George, S. M. *Chem. Rev.* **2010**, *110*, 111−131.
(2) Du, Y.; George, S. M. *J. Phys. Chem. C* **2007**, *111*, 8509−8517.
(3) George, S. M.; Lee, B. H.; Yoon, B.; Abdulagatov, A. I.; Hall, R. A. *J. Nanosci. Nanotechnol.* **2011**, *11*, 7948−7955.
(4) Chujo, Y. *Curr. Opin. Solid State Mater. Sci.* **1996**, *1*, 806−811.
(5) Judeinstein, P.; Sanchez, C. *J. Mater. Chem.* **1996**, *6*, 511−525.
(6) Yoon, B.; Lee, B. H.; George, S. M. *J. Phys. Chem. C* **2012**, *116*, 24784−24791.
(7) Adamczyk, N. M.; Dameron, A. A.; George, S. M. *Langmuir* **2008**, *24*, 2081−2089.
(8) Dameron, A. A.; Seghete, D.; Burton, B. B.; Davidson, S. D.; Cavanagh, A. S.; Bertrand, J. A.; George, S. M. *Chem. Mater.* **2008**, *20*, 3315−3326.
(9) Peng, Q.; Gong, B.; VanGundy, R. M.; Parsons, G. N. *Chem. Mater.* **2009**, *21*, 820−830.
(10) Yoon, B.; O'Patchen, J. L.; Seghete, D.; Cavanagh, A. S.; George, S. M. *Chem. Vap. Depos.* **2009**, *15*, 112−121.
(11) Yoon, B.; Seghete, D.; Cavanagh, A. S.; George, S. M. *Chem. Mater.* **2009**, *21*, 5365−5374.
(12) Seghete, D.; Hall, R. A.; Yoon, B.; George, S. M. *Langmuir* **2010**, *26*, 19045−19051.
(13) Gong, B.; Peng, Q.; Parsons, G. N. *J. Phys. Chem. B* **2011**, *115*, 5930−5938.
(14) Huang, X.; Roushan, M.; Emge, T. J.; Bi, W.; Thiagarajan, S.; Cheng, J.-H.; Yang, R.; Li, J. *Angew. Chem., Int. Ed.* **2009**, *48*, 7871−7874.
(15) Chen, Y.-C.; Yao, H.; Thiagarajan, S.; Wu, M.; Emge, T. J.; Yang, R.; Yu, S.; Li, J. *Z. Anorg. Allg. Chem.* **2012**, *638*, 2604−2609.
(16) Wu, M.; Rhee, J.; Emge, T. J.; Yao, H.; Cheng, J.-H.; Thiagarajan, S.; Croft, M.; Yang, R.; Li, J. *Chem. Commun.* **2010**, *46*, 1649−1651.
(17) Costescu, R. M.; Cahill, D. G.; Fabreguette, F. H.; Sechrist, Z. A.; George, S. M. *Science* **2004**, *303*, 989−990.
(18) Li, Z.; Tan, S.; Bozorg-Grayeli, E.; Kodama, T.; Asheghi, M.; Delgado, G.; Panzer, M.; Pokrovsky, A.; Wack, D.; Goodson, K. E. *Nano Lett.* **2012**, *12*, 3121−3126.
(19) Yoneoka, S.; Lee, J.; Liger, M.; Yama, G.; Kodama, T.; Gunji, M.; Provine, J.; Howe, R. T.; Goodson, K. E.; Kenny, T. W. *Nano Lett.* **2012**, *12*, 683−686.
(20) Patterson, A. L. *Phys. Rev.* **1939**, *56*, 978−982.
(21) Cahill, D. G. *Rev. Sci. Instrum.* **2004**, *75*, 5119−5122.
(22) Schmidt, A. J.; Chen, X.; Chen, G. *Rev. Sci. Instrum.* **2008**, *79*, 114902−114909.
(23) Liu, J.; Zhu, J.; Tian, M.; Gu, X.; Schmidt, A.; Yang, R. *Rev. Sci. Instrum.* **2013**, *84*, 034902.
(24) Hostetler, J. L.; Smith, A. N.; Morris, P. M. *Int. J. Thermophys.* **1998**, *19*, 569−577.
(25) Zhu, J.; Tang, D. W.; Wang, W.; Liu, J.; Holub, K. W.; Yang, R. G. *J. Appl. Phys.* **2010**, *108*, 094315.
(26) Henry, A.; Chen, G. *Phys. Rev. Lett.* **2008**, *101*, 235502−235504.
(27) Liu, J.; Yang, R. *Phys. Rev. B* **2012**, *86*, 104307.
(28) Xu, Y.; Goto, M.; Kato, R.; Tanaka, Y.; Kagawa, Y. *J. Appl. Phys.* **2012**, *111*, 084320−7.
(29) Brydson, J. A. *Plastics Materials*, 7th ed.; Butterworth-Heinemann: Oxford, 1999; pp 59−75.
(30) Losego, M. D.; Grady, M. E.; Sottos, N. R.; Cahill, D. G.; Braun, P. V. *Nat. Mater.* **2012**, *11*, 502−506.
(31) Losego, M. D.; Blitz, I. P.; Vaia, R. A.; Cahill, D. G.; Braun, P. V. *Nano Lett.* **2013**, *13*, 2215−2219.
(32) Ong, W.-L.; Rupich, S. M.; Talapin, D. V.; McGaughey, A. J. H.; Malen, J. A. *Nat. Mater.* **2013**, *12*, 410−415.
(33) Kittel, C. *Introduction to Solid State Physics*, 8th ed.; Wiley: New York, 2004.
(34) Ashcroft, N. W.; Mermin, N. D. *Solid State Physics*; Brooks/Cole: Independence, 1976.
(35) Liu, J.; Alhashme, M.; Yang, R. *Carbon* **2011**, *50*, 1063−1070.
(36) Wunderlich, B. *Pure Appl. Chem.* **1995**, *67*, 1019−1026.
(37) Harper, C. A. *Modern Plastics Handbook*; McGraw Hill Professional: New York, 2000.
(38) Seko, A.; Oba, F.; Kuwabara, A.; Tanaka, I. *Phys. Rev. B* **2005**, *72*, 024107.
(39) Lee, S. M.; Cahill, D. G.; Allen, T. H. *Phys. Rev. B* **1995**, *52*, 253−257.
(40) Cahill, D. G.; Goodson, K.; Majumdar, A. *J. Heat Trans.* **2002**, *124*, 223−241.